

Incorporating climate change and morphological uncertainty into coastal change hazard assessments

Heather M. Baron · Peter Ruggiero · Nathan J. Wood ·
Erica L. Harris · Jonathan Allan · Paul D. Komar · Patrick Corcoran

Received: 25 October 2013 / Accepted: 1 September 2014 / Published online: 13 September 2014
© The Author(s) 2014. This article is published with open access at Springerlink.com

Abstract Documented and forecasted trends in rising sea levels and changes in storminess patterns have the potential to increase the frequency, magnitude, and spatial extent of coastal change hazards. To develop realistic adaptation strategies, coastal planners need information about coastal change hazards that recognizes the dynamic temporal and spatial scales of beach morphology, the climate controls on coastal change hazards, and the uncertainties surrounding the drivers and impacts of climate change. We present a probabilistic approach for quantifying and mapping coastal change hazards that incorporates the uncertainty associated with both climate change and morphological variability. To demonstrate the approach, coastal change hazard zones of arbitrary confidence levels are developed for the Tillamook County (State of Oregon, USA) coastline using a suite of simple models and a range of possible climate futures related to wave climate, sea-level rise projections, and the frequency of major El Niño events. Extreme total water levels are

H. M. Baron · P. Ruggiero (✉) · E. L. Harris · P. D. Komar · P. Corcoran
College of Earth, Ocean, and Atmospheric Sciences, Oregon State University, Corvallis, OR 97331,
USA
e-mail: pruggier@coas.oregonstate.edu

Present Address:

H. M. Baron
Coastal Monitoring and Analysis Program, Washington State Department of Ecology, Olympia,
WA 98504, USA
e-mail: hbar461@ecy.wa.gov

N. J. Wood
Western Geographic Science Center, U.S. Geological Survey, Portland, OR, USA
e-mail: nwood@usgs.gov

Present Address:

E. L. Harris
AECOM, Oakland, CA, USA

J. Allan
Oregon Department of Geology and Mineral Industries, Newport, OR 97365, USA
e-mail: jonathan.allan@dogami.state.or.us

more influenced by wave height variability, whereas the magnitude of erosion is more influenced by sea-level rise scenarios. Morphological variability has a stronger influence on the width of coastal hazard zones than the uncertainty associated with the range of climate change scenarios.

Keywords Climate change · El Niño · Exposure · Increasing storminess · Probabilistic coastal hazard zones · Sea-level rise · Uncertainty

1 Introduction

Sea-level rise (SLR), increasing storminess, and development pressures all contribute to making coastal communities vulnerable to coastal change hazards (e.g., Bindoff et al. 2007; Young et al. 2011; Strauss et al. 2012). A significant challenge for coastal planners in reducing this vulnerability is the lack of tools or information that recognize the inherent uncertainty of climate change and its influence on physical processes that shape the coastal zone. Although they are the basis for coastal policies, regulations, and adaptation planning efforts, many coastal change hazard mapping efforts (e.g., Allan and Priest 2001) effectively ignore the non-stationarity of coastal processes, such as accelerating SLR and changes in storminess.

Forecasts of potential impacts to coastal areas due to climate change and/or extreme events have been performed on the US West Coast using qualitative indices (Thieler and Hammar-Klose 1999); quantitative, event-selection or benchmark event approaches (e.g., Allan and Priest 2001); and response-based or structural function approaches (Revell et al. 2011). Fully probabilistic, full temporal simulation approaches that account for conditional dependencies between relevant variables (e.g., Callaghan et al. 2008) are considered the most robust and involve randomly sampling from fitted probability distributions in a Monte Carlo sense. Both the response function and full simulation approaches have the potential to include the non-stationarity associated with climate change.

In addition to the variability in physical processes, community exposure to coastal change hazards varies depending on how communities currently use or plan to use hazard-prone areas. There have been various efforts in recent years to estimate societal exposure to various SLR scenarios throughout the world (e.g., Wu et al. 2009; Strauss et al. 2012), as well as efforts to estimate the influence of SLR in increasing societal exposure to sudden-onset coastal hazards, such as hurricane storm surge (e.g., Frazier et al. 2010). Lacking from these studies are attempts to characterize community vulnerability to coastal change hazards, such as chronic erosion associated with winter storms.

Within this context of hazard uncertainty and societal relevance, the objective of this paper is to summarize a multi-scale, probabilistic methodology that incorporates the impacts of projected climate changes and variability, as well as morphological variability, into coastal change hazard assessments. We first develop a suite of climate change scenarios that reflect various assumptions regarding SLR, storminess, and major El Niño occurrences and their impact on future extreme water levels. Simple models are then used to quantify potential coastal change hazards and generate a series of probabilistic hazard zones for select events over a range of timescales (event to decadal) that account for both climate and morphological uncertainties. We integrate these hazard zones with data on local infrastructure to examine spatial variations in community exposure to coastal change hazards. Finally, we examine the

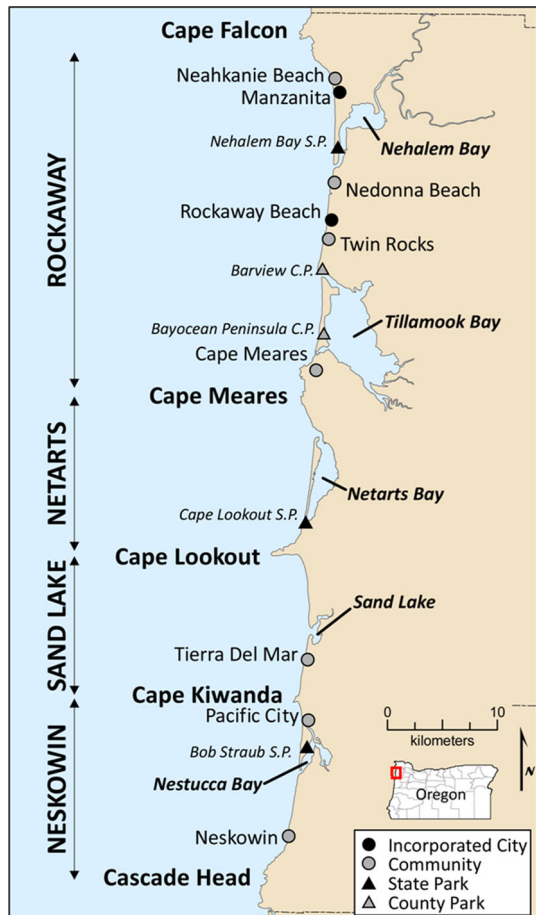
relative contribution of sea level, wave climate, and the frequency of occurrence of major El Niños to the magnitude and spatial extent of coastal change hazard zones.

To demonstrate this integrated approach, we focus on the multiple coastal communities and littoral cells along dune-backed shorelines in Tillamook County on the northern coast of Oregon (USA). Although we focus on one county and its littoral cells, the methodology is applicable to all dune-backed shorelines in the US Pacific Northwest [covering approximately 45 % of the outer coasts of Oregon and Washington (Cooper 1958)], as well as other coastal regions with similar physical settings. Methods presented here further the dialogue on understanding community exposure to coastal change hazards that incorporate climate change uncertainty and can be used by coastal planners in their efforts to balance community growth and increased adaptive capacity to natural hazards over the next several decades.

2 Study area

Coastal Tillamook County in northwest Oregon contains four littoral cells separated by bounding headlands (Fig. 1). Each littoral cell is further divided by at least one estuary.

Fig. 1 Map of the four littoral cells of Tillamook County, OR, as divided by five major headlands, showing the coastal communities, estuaries, and recreational parks along the coast



Two of the littoral cells have inlets stabilized by jetties (Tillamook Bay and Nehalem Bay), whereas the mouths of the other estuaries are free to migrate and shift in response to hydrodynamic forcing, as the sediment budget allows. The Rockaway littoral cell is the largest and most densely populated in the study area with several tourism-driven communities located along 25 km of shoreline. The focus in the Netarts littoral cell is the 7.5-km-long Netarts Spit that includes Cape Lookout State Park, which has been experiencing significant dune erosion and dune overtopping during the last few decades. The Sand Lake littoral cell is largely uninhabited, aside from the small community of Tierra Del Mar. At the southern end of the study area, the Neskowin littoral cell has experienced shoreline progradation in the northern section (e.g., near Pacific City) and significant erosion in the southern part. The erosion, averaging about 2.0 m per year since the 1960s (Ruggiero et al. 2013), is threatening oceanfront residences in the community of Neskowin.

The dynamic beaches of Tillamook County, OR, are exposed to mesotidal conditions and a relatively extreme wave climate. Monthly mean significant wave heights off the coast of Oregon are on the order of 1.5 m in the summer with periods of ~ 8 s, while wave heights in the winter are typically double in height, averaging ~ 3 m with periods on the order of 12–13 s (Ruggiero et al. 2005). It is typical for winter storms to annually generate wave heights >10 m, while some of the strongest storms on record have generated waves up to 14 m (Allan and Komar 2002, 2006). Peak periods associated with these large wave heights tend to be about 15–17 s, but can be as large as 20 s (Allan and Komar 2002). The strong seasonal variability in water levels, ~ 20 cm (Komar et al. 2011), is in phase with the seasonal variability in the wave climate, resulting in significantly higher total water levels (TWLs) during the winter season. During major El Niño events, water levels, wave heights, and wave direction are all anomalous, resulting in regional and hotspot erosion throughout the region.

3 Climate change scenario development

Climate change scenarios serve as the foundation for the coastal change hazard zones and are based on the projections for SLR, the wave climate, and the probability of occurrence of major El Niño events through the year 2100. Due to the inherent uncertainty in climate projections (e.g., Hemer et al. 2013), our approach here is to broadly explore the range of variability documented in the literature rather than dynamically or statistically downscaling the various processes from models (Wilby and Dessai 2012).

The SLR projections were made by compiling estimates based on semiempirical methods (e.g., Rahmstorf 2010) relating SLR to the global mean temperature for the IPCC SRES scenario A1B. We integrate the uncertainty associated with the various A1B SLR projections by fitting a quadratic equation to several high, medium, and low estimates and then bracket the uncertainty associated with our A1B scenarios with a fitted “best-case” B1 scenario and fitted “worst-case” A2 scenario. Estimates range from 0.45 to 1.47 m of SLR by 2100 relative to 2010 (Fig. 2a), a range of SLR projections comparable to those presented in a recent report from the National Research Council specific to the US West Coast (NRC 2012). Relative SLR scenarios relevant to the US Pacific Northwest were determined by correcting the global SLR projections to account for processes that locally alter sea-level projections, such as alongshore variations in land uplift rates due to the subduction of the oceanic Juan de Fuca and Gorda plates under the continental North American plate (e.g., Burgette et al. 2009; Komar et al. 2011).

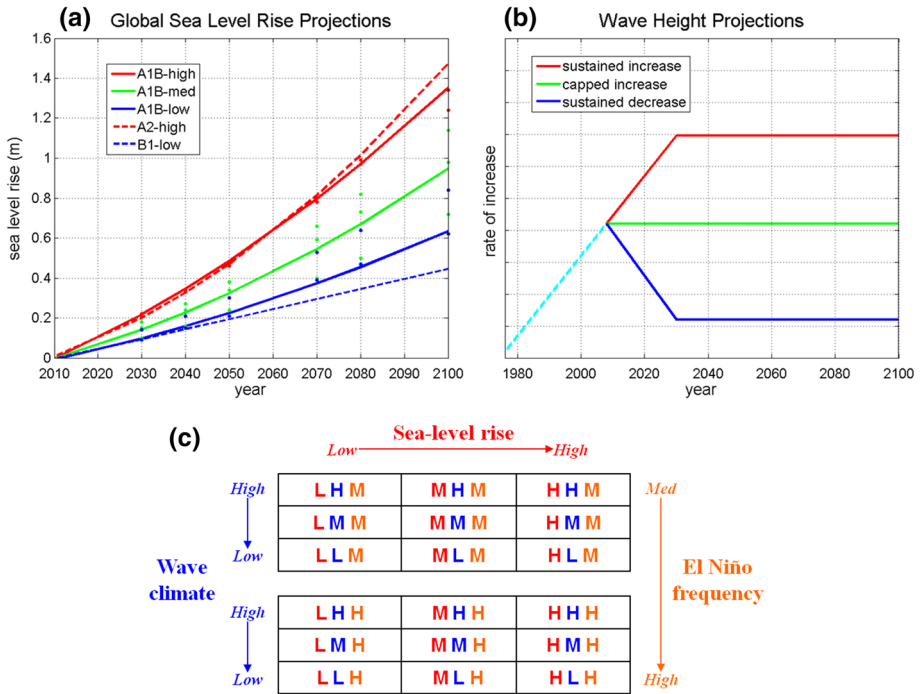


Fig. 2 a SLR, b wave climate, and El Niño projections combine to generate an initial matrix of c 18 initial climate change scenarios for use in coastal change models. We further combine the B1-low SLR estimate with the decreased intensity wave climate and no increase in El Niños and combine the A2-high SLR estimate with the increased intensity wave climate and the doubling of El Niño frequency for a total of 20 scenarios covering a broad range of possible climate futures

The extreme wave height climatology has been documented to be increasing over the last few decades (Allan and Komar 2000, 2006; Méndez et al. 2006; Menéndez et al. 2008; Ruggiero et al. 2010; Young et al. 2011), and this increase has been potentially more responsible than changes in sea level alone for increasing the frequency of extreme events along the PNW coast (Ruggiero 2013). Moreover, wave heights of different magnitudes (i.e., exceedance percentiles) are increasing at different rates such that larger waves are getting bigger faster (Ruggiero et al. 2010). Therefore, wave heights in our future wave climate scenarios were allowed to change by quartile, depending on their exceedance percentile of the wave height cumulative distribution function. We developed three simple future wave climate scenarios: (1) wave heights increase at their present rate of 1.0, 1.5, 2.0, or 4.0 cm/year, depending on quartile, as documented by Ruggiero et al. (2010) until 2030; (2) wave heights remain at their present levels indefinitely; and (3) wave heights decrease until the year 2030 at the same rate as the wave height increase scenario (Fig. 2b). We extend our wave scenarios only for two decades due to the lack of a detailed understanding of the causation of the existing trends, and the uncertainty associated with downscaling winds and waves from model projections (e.g., Hemer et al. 2013).

Major El Niños significantly affect both water levels and wave heights in the PNW and have been associated with the most severe erosion and flooding hazards in the region documented over the last few decades (Kaminsky et al. 1998). Over the period of wave

buoy measurements, there have been two major El Niños—one in 1982–1983 and another in 1997–1998. Because little is certain about how El Niño frequency will change in the future, we include one scenario in which the frequency of occurrence of major El Niños doubles to approximately two per 15 years. Recent modeling work (Cai et al. 2014) has suggested that a scenario of increased frequency of major El Niños due to greenhouse warming is plausible. The additional El Niños are added by increasing water levels and wave heights over the course of entire winters, to match the scale of the event during the winter of 1997–1998. For comparison, we also develop a scenario in which the frequency of El Niños remains the same as during the last several decades. Combining these SLR, wave climate, and El Niño projections, we generate 20 climate change scenarios, covering a broad range of climate uncertainty (Fig. 2c). In this application, we assume that each climate change scenario has an equal probability of occurrence (i.e., a rectangular probability density function); however, it is straightforward to assess the impacts of an imposed occurrence probability distribution function if warranted.

4 Defining coastal change hazard zones

Existing coastal change hazard zones in Oregon (e.g., Allan and Priest 2001) were developed deterministically with an event-selection approach that includes an assessment of the TWL and the application of a simple geometric dune erosion model (Komar et al. 1999, hereafter K99). We extend this work with a probabilistic treatment to evaluate the influence of climate change and morphological change uncertainty on expected coastal change hazards. A general expression for a coastal change hazard zone (CCHZ) can be expressed as:

$$\text{CCHZ} = (\text{CCR}_{\text{SB}} + \text{CCR}_{\text{climate}})T + \text{CC}_{\text{event}} + \text{CC}_{\text{HS}} \quad (1)$$

where CCR_{SB} is the long-term (interannual to decadal scale) coastal change rate associated with sediment budget factors not influenced by climate change (e.g., changes in sediment supply due to engineering structures) and $\text{CCR}_{\text{climate}}$ is the coastal change rate associated with climate change-induced factors as expressed through the TWL. In many applications, SLR will be the major component of this term but other factors that can influence TWL trends can be included, such as increasing wave setup due to increasing wave heights or climate-induced trends in storm surge. T is the time period of interest for the CCHZ, typically on the order of several decades. Conservatism is built into the approach by the inclusion of erosion associated with a significant (extreme) storm event, CC_{event} , added to the long-term changes. In the case of increasing wave height scenarios, this approach allows us to incorporate non-stationarity into analyses of the extremes. For example, the 100-year return level storm event in 2030 may be very different than the 100-year storm event in 2011 (Ruggiero et al. 2010). The inclusion of the parameter CC_{HS} attempts to account for localized erosion due to processes that are difficult to resolve over large areas, such as rip current embayments or hotspot erosion impacts during El Niños. Here, we ignore the terms CCR_{SB} and CC_{HS} because they are typically poorly known and difficult to model; however, they can easily be incorporated in future efforts as more sophisticated tools become available.

The influence of SLR on $\text{CCR}_{\text{climate}}$ is characterized with a simple “Bruun Rule” type calculation (Bruun 1962), which provides order-of-magnitude estimates of the retreat of unprotected coastlines due to SLR via mass conservation in the absence of significant

sediment sources and sinks. Given a rise in sea level, S , the amount of landward shoreline retreat, $CC_{climate}$, is found using

$$CC_{climate} = \frac{L}{B + h} S = \frac{S}{\tan \beta_{sf}} \tag{2}$$

where L is the cross-shore distance to the water depth, h is the depth beyond which significant gradients in sediment transport do not occur (the closure depth), and B is the elevation of an onshore feature (such as a beach berm) or a shoreline contour. The term $L/(B + h)$ is equivalent to the inverse of shoreface slope, $\tan \beta_{sf}$. As sea level rises, the shoreface slope is assumed to remain constant while the dune toe elevation becomes higher relative to the land. Coastal retreat can also take place during large storm events or periods of elevated water levels in the form of wave-induced, foredune erosion, in which the magnitude of erosion depends on the elevation of the TWL relative to the toe of the foredune (Sallenger 2000; Ruggiero et al. 2001; Stockdon et al. 2006). The TWL is defined as:

$$TWL = \bar{\eta} + \eta_a + \eta_r + R \tag{3}$$

where $\bar{\eta}$ is the time-averaged water level or mean sea level, η_a is the astronomical tide level, and η_r is the non-tidal residual water level (i.e., storm surge and other oceanographic processes that raise or lower water levels). These three factors make up the measured tidal elevation, E_T , and are added to the wave run-up (R). Run-up is composed of both setup and swash, here calculated using the 2 % exceedance value of swash maxima as defined by an empirical relation for extreme wave run-up by Stockdon et al. (2006).

When these substitutions are made, the TWL equation becomes

$$TWL = E_T + 1.1 \left(0.35 \tan \beta_{bs} (H_0 L_0)^{1/2} + \frac{[H_0 L_0 (0.563 \tan \beta_{bs}^2 + 0.004)]^{1/2}}{2} \right) \tag{4}$$

where $\tan \beta_{bs}$ is the beach slope, H_0 is the deepwater significant wave height, and L_0 is the deepwater wave length, given as $(g/2\pi)T^2$ where g is the acceleration due to gravity and T is the peak wave period. This formula is applicable over a variety of beach conditions, ranging from dissipative to reflective, and thus suitable for all dune-backed beaches in the study area. Because the focus here is on extreme TWLs, in which run-up can occur over the entire beach face, the backshore beach slope is used and is defined as the slope between the mean high water (MHW) shoreline contour and the dune toe.

To statistically determine extreme TWLs for the annual and 100-year return level at each time period of interest, we use the peak-over-threshold method of extreme value theory (Coles 2001) that requires a high threshold and models exceedances over this threshold. We assume that the number of exceedances in a given year follows a Poisson distribution and that the threshold excesses are modeled using the generalized Pareto distribution. The threshold value is set such that, on average, five TWL events per year are analyzed, a value equal to about the 97–98th exceedance percentile of the overall TWL climatology. While this application of extreme value theory assumes stationarity in the TWL time series, climate change-induced trends in the TWL are accounted for by calculating extreme values separately for each time period of interest.

Waves begin to impact dunes and erosion occurs when the TWL exceeds the elevation of the dune toe during extreme events. To quantify the amount of coastal change that can take place during a period of elevated TWLs, we apply the simple K99 geometric foredune

erosion model that assumes a dune toe will retreat upward and landward as a function of the maximum TWL experienced during a large event, while maintaining a constant backshore beach slope. The maximum expected storm-induced dune erosion, DE_{\max} , is calculated as

$$DE_{\max} = \frac{TWL - E_J}{\tan \beta_{bs}} \quad (5)$$

where E_J is the elevation of the junction between the dune and the upper beach, or the toe of the dune. The K99 dune erosion model is typically fairly conservative (Mull and Ruggiero 2014) and likely overpredicts the amount of erosion that might actually occur during a single storm event. Other event-scale coastal change models can be used if the necessary input data are available (e.g., dune height, sediment grain size, surf zone width, breaking wave depth, and storm duration), such as the equilibrium dune erosion model of Kriebel and Dean (1993) or the wave impact model of Larson et al. (2004).

To account for the long-term effect of SLR which acts to move the dune toe elevation landward and upward, E_J is adjusted by the change in sea level, S , that occurs over the time period of interest so that for the application presented here, the amount of coastal change that takes place during, for example, the annual or 100-year return TWL event is

$$CC_{\text{event}} = \frac{TWL_{\text{event}} - (E_J + S)}{\tan \beta_{bs}} \quad (6)$$

In the case of the increasing wave height scenarios, the approach outlined here incorporates non-stationarity into the analyses of the extremes.

5 Morphometric and hydrodynamic inputs

Shoreface slopes, $\tan \beta_{sf}$, which are inputs to Bruun Rule calculations, were estimated by calculating the slope between the approximate multidecadal depth of closure and the MHW shoreline (2.1 m contour, relative to NAVD88), derived from lidar data. Nearshore bathymetry was extracted at 500-m alongshore intervals from a 6 arc-second digital elevation map (NOAA Center for Tsunami Research 2004). The 20-m isobath was chosen for estimating shoreface slopes; however, results were fairly insensitive to a range of reasonable values (15–25 m). The 500-m resolution of alongshore varying shoreface slopes was interpolated to match the more highly resolved- and variable-beach morphometrics. The remaining morphometric parameters were derived from high-resolution lidar data collected in September 2002 (NOAA Coastal Services Center 2002) and are summarized in Mull and Ruggiero (2014), where dune toe elevation and backshore beach slope were defined for thousands of cross-shore profiles every few meters along the southwest Washington and Oregon coastlines.

We account for beach and dune morphometric variability by randomly sampling dune toe elevations and beach slopes from distributions. Using the highly resolved spatial variability in the lidar dataset as a proxy for temporal variability [following the approach of Ruggiero and List (2009)], the backshore beach slope is allowed to vary by randomly sampling from a normal distribution defined by the median and standard deviation of 1-km shoreline segments in each littoral cell. Beach level variations due to rip current embayments are indirectly accounted for by incorporating the spatial variability within a 1-km

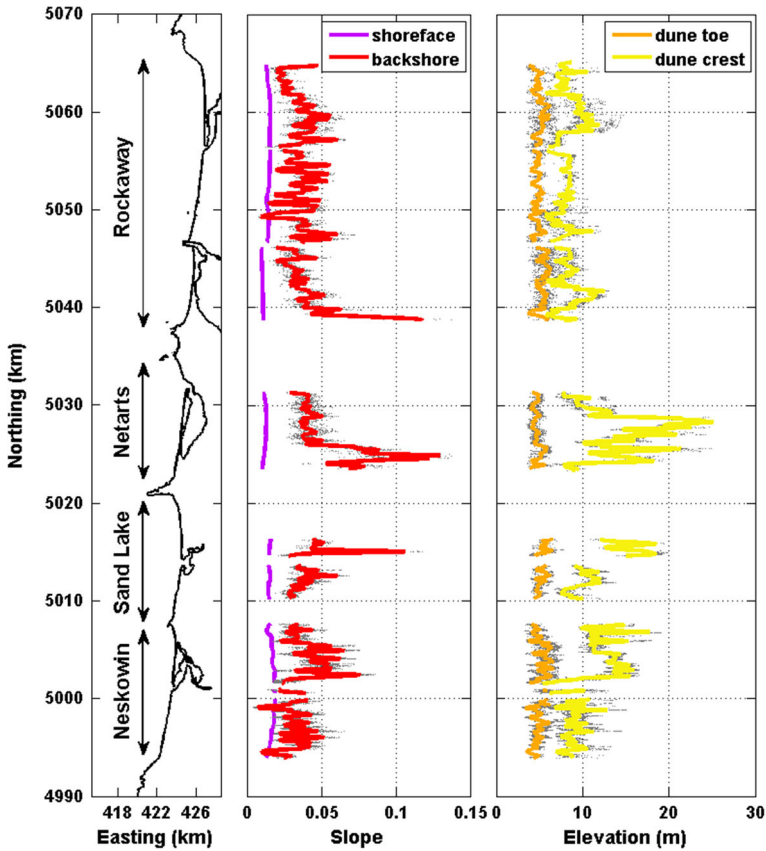


Fig. 3 Alongshore varying morphometrics for dune-backed beaches in Tillamook County, OR. For each parameter, the *gray dots* represent the raw data while the *colored lines* are the values smoothed in the alongshore direction to eliminate variability less than 250 m using a quadratic loess filter (Plant et al. 2002)

stretch of shoreline. Dune toe elevations are normally distributed where the mean is the lidar-derived value, and the standard deviation is defined by the vertical error associated with its selection and interpolation, mean total RMSE = 0.66 m (Mull and Ruggiero 2014). One hundred random dune toe and beach slope configurations were combined with each of the 20 climate change scenarios, resulting in 2,000 computations of storm-induced coastal change at each of the lidar-derived profiles.

In Tillamook County, the beach and foredune morphology varies both within and among the four littoral cells (Fig. 3). The mean and standard deviation of the relevant parameters extracted from the 2002 lidar data are summarized in Table 1. The dune toe and dune crest elevations averaged for the entire county are approximately 5 and 11 m, respectively. The dune-backed beaches in the Netarts littoral cell have the highest mean dune crest elevation (13.6 ± 4.1 m) but one of the lowest mean dune toe elevations (4.8 ± 0.6 m), suggesting that while these dunes are relatively more susceptible to wave-induced erosion, they may not be as likely to overtop. The smallest dunes are found in the Rockaway littoral cell, where the average dune crest elevation is 8.4 ± 1.7 m, though the dune toe elevation is slightly above the county average at 5.2 ± 0.8 m.

Table 1 Mean and standard deviations (SD) of beach and foredune parameters for the littoral cells of Tillamook County, Oregon, relative to NAVD88, as extracted from 2002 lidar data (Mull and Ruggiero 2014)

Littoral cell	Shoreface slope		Backshore slope		Dune toe elev. (m)		Dune crest elev. (m)	
	Mean	SD	Mean	SD	Mean	SD	Mean	SD
Rockaway	0.013	0.002	0.037	0.01	5.2	0.8	8.4	1.7
Netarts	0.013	0.001	0.051	0.02	4.8	0.6	13.6	4.1
Sand Lake	0.015	0.001	0.041	0.01	5.2	0.7	11.7	3.3
Neskowin	0.017	0.001	0.037	0.01	5.1	0.9	10.8	2.7
County-wide	0.015	0.003	0.039	0.01	5.1	0.8	10.7	3.2

After characterizing the local morphology, wave and water-level time series are generated so that extreme TWLs can be calculated as input conditions to the coastal change models. A combined time series is first produced that synthesizes data from wave buoys in the region (NDBC 2007) to develop as complete a significant wave height and spectral peak period record as possible (following Allan et al. 2012). The wave record is then joined with the Newport, Oregon tide gauge record, which dates back to the mid-1960s (NOAA 2007). Following the methods described in Ruggiero et al. (2001), we generate an hourly TWL time series by combining hourly estimates of run-up with hourly tide gauge measurements (Eq. 3). Since the wave run-up model depends on local beach slope, separate TWL time series are developed for all possible beach slopes relevant to our study region. For our north-central Oregon coast study site, the joint time series extends from 1976 to 2009 and is approximately 85 % complete due to data gaps.

Extreme value theory is then applied to the joint time series to develop design conditions relevant for present-day conditions, i.e., the annual and 100-year return level TWL. By definition, the annual event has on a 100 % chance of occurring every year, while the 100-year event, representing a much larger, and more rare, storm with a higher TWL, has a 1 % chance of occurring every year. We construct 20 projected TWL time series (per representative beach slope)—one for each of the 20 climate change scenarios. The projected TWL time series are extended through the year 2100 by repeating the observed time series approximately three times and incorporating non-stationarity by applying the climate change scenarios to the wave height and water-level components of the TWL. These synthetic TWL time series allow us to compute extreme design conditions at any time over the next century (e.g., 2030, 2050, and 2100) for each scenario, covering a broad range of climate change variability.

Because the extreme TWLs vary smoothly across the range of beach slopes, lookup tables of the extreme values through time are developed to interpolate extreme TWL values for any slope. For the 20 climate change scenarios and 100 combinations of slope and dune toe parameters, 2,000 sets of extreme TWLs for each event at each time period of interest are calculated by interpolating from the lookup tables. The resulting extreme TWLs were used in conjunction with the derived morphometrics to quantify future coastal change hazards.

Extreme TWL values for the annual and 100-year events in 2009, 2030, 2050, and 2100 were calculated for a range of backshore beach slopes for each of the 20 climate change scenarios (Eq. 4). Extreme TWLs vary depending on the local beach slope, where TWLs reach higher elevations on steeper beaches (Fig. 4). As the magnitude of extreme TWL

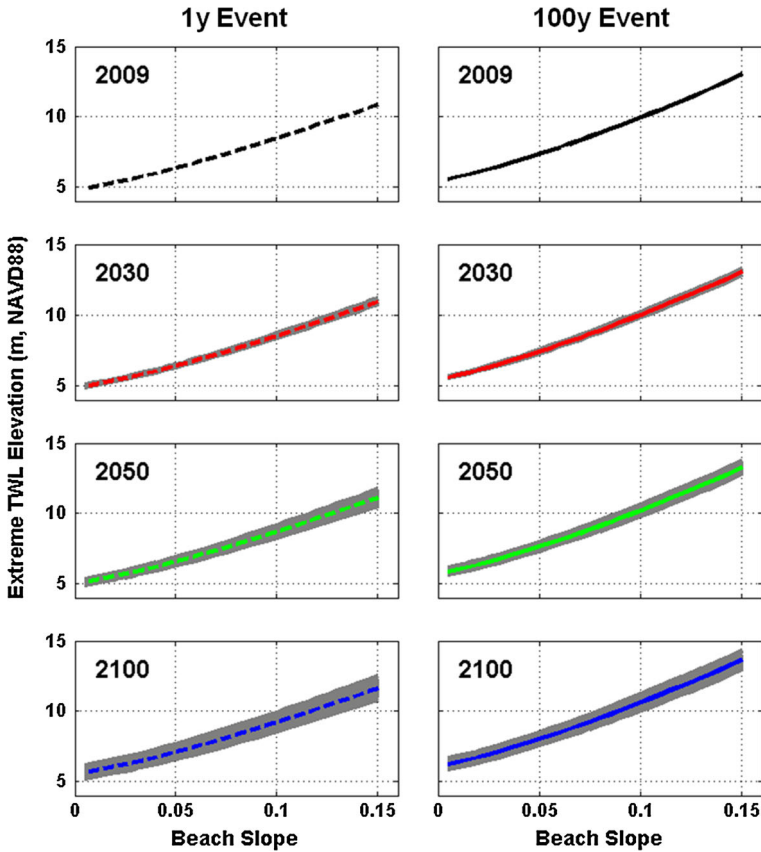


Fig. 4 Uncertainty range of extreme TWL elevations, in meters, over a range of backshore beach slopes through time, for both the annual (*left*) and 100-year (*right*) TWL events. The *gray areas* represent the uncertainty or range of TWLs given the 20 climate change scenarios, while the *dark colored lines* show the mean values

events increases through time, the uncertainty in those TWLs also increases due to the increasing uncertainty associated with each of the climate change components (Fig. 4).

At each of the cross-shore profiles in Tillamook County, for all 100 configurations of morphology, the annual and 100-year return level event TWL elevations were interpolated from the extreme TWL curves generated for each of the 20 climate change scenarios. Figure 5 illustrates the alongshore varying mean TWLs for the Neskowin littoral cell in 2009 as compared to the present-day (2002) dune toe and dune crest elevations. The mean TWL is greater than the elevation of the dune toe in almost all cases—79 % (98 %) of the time for the annual (100-year) event—indicating that some amount of storm-induced coastal change associated with these two extreme TWL events is likely under present-day conditions, even before any amount of additional SLR occurs. When averaged across all littoral cells, the 100-year TWL event is found to be ~0.9 m larger than the annual event. Throughout the century, the highest TWLs are experienced in the Netarts littoral cell because it contains the steepest backshore slopes. On average, the TWLs increase by

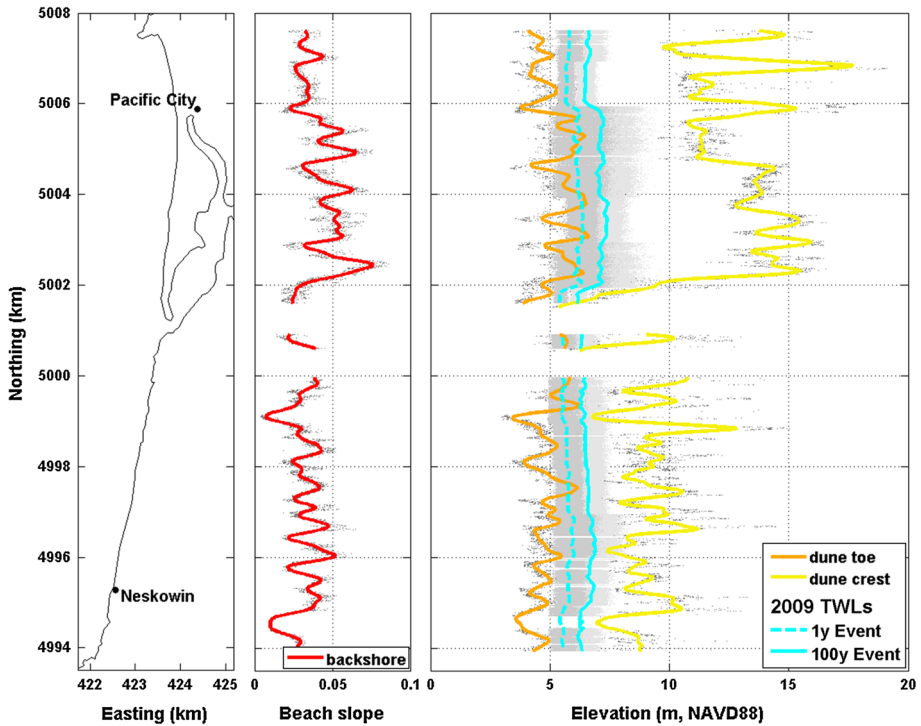


Fig. 5 Example of extreme TWLs for the Neskowin littoral cell in 2009. The *left panel* shows the shoreline and location of two coastal communities in the littoral cell. The alongshore varying beach slopes (*red*) are shown in the *middle panel*. The *right panel* shows the mean TWLs (*cyan*) for the annual (*dashed*) and 100-year (*solid*) events as compared to the dune toe (*orange*) and dune crest (*yellow*) elevations

~0.7 m from 2009 to 2100 for the both the annual and 100-year TWL events, corresponding to a 10–12 % increase.

6 Magnitude of coastal change

The total magnitude of potential coastal change estimated for each cross-shore profile results from a combination of the projected shoreline retreat associated with rising sea levels (CC_{climate}) and the maximum expected wave-induced foredune erosion in response to a given extreme TWL event (CC_{event}). We first examine how these two components combine to produce the total predicted coastal change by quantifying them individually. Figure 6 illustrates the retreat distances associated with the three SLR scenarios, the alongshore varying mean of the 2,000 estimates for the 100-year TWL event, and the mean total estimate of potential erosion for the Neskowin littoral cell in 2050. For this time period, the expected mean dune erosion caused by this extreme TWL event (Eq. 6) is greater than the shoreline retreat associated with both the low and medium SLR (Eq. 2). When these variables are summated in both the cross-shore and alongshore to compute an overall mean and standard deviation associated with each erosion component, the overall mean for CC_{climate} is shown to be only half that for CC_{event} (17.9 vs. 36.3 m). The

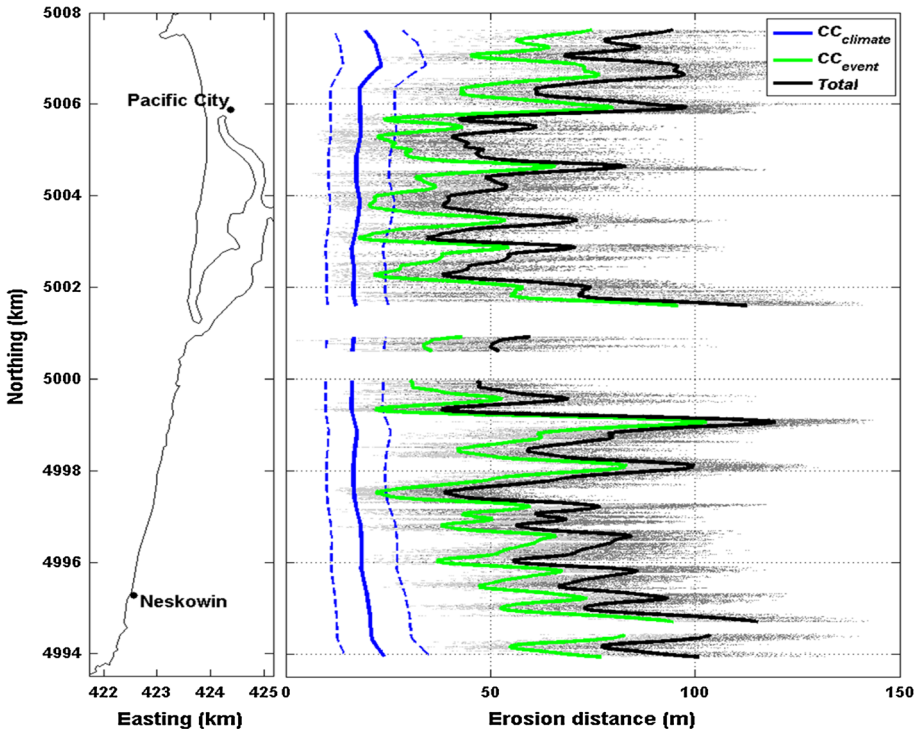


Fig. 6 Example of alongshore varying mean coastal retreat distances associated with the 100-year TWL event in 2050 for the Neskowin littoral cell, in meters. The *panel on the right* shows the potential retreat associated with the low, medium, and high SLR scenarios for $CC_{climate}$ (blue; from left to right), CC_{event} (green), as well as the total predicted mean retreat (black)

alongshore variability in the total mean coastal change is influenced most by the variability in CC_{event} , which exhibits much greater alongshore variability than $CC_{climate}$, as a direct result of the variability in the morphological parameters from which each of the terms is calculated ($\tan \beta_{bs}$ and E_j vs. $\tan \beta_{sf}$).

Though it varies slightly between littoral cells, the difference in magnitude of total coastal change forecasted between the annual and 100-year TWL events for any time period of interest is ~ 17 m (Eq. 6). The Neskowin littoral cell is forecasted to have the least amount of shoreline retreat due to increasing sea levels, as it has the steepest shoreface slopes ($\tan \beta_{sf}$) of the county (Eq. 2). However, because there are many areas of relatively flat beaches backed by foredunes with low dune toes, it is estimated to experience the greatest amount of event-based coastal dune erosion throughout the century.

In 2009, 100 % of the CCHZ is attributed to storm-induced erosion of the foredune associated with a given extreme TWL event (Eq. 6). When averaged across the four littoral cells, CC_{event} is responsible for about 33 m (50 m) of erosion associated with the annual (100-year) TWL event in 2009 (Eq. 6). As the century progresses, this magnitude stays relatively constant, increasing by only 0.5–1 m even though the waves are allowed to increase/decrease until 2030. Shoreline retreat associated with rising sea levels ($CC_{climate}$), however, starts at 0 m in 2009 and increases to ~ 50 – 70 m in 2100, depending on the littoral cell (Eq. 2). As the magnitude of $CC_{climate}$ increases, so does its relative

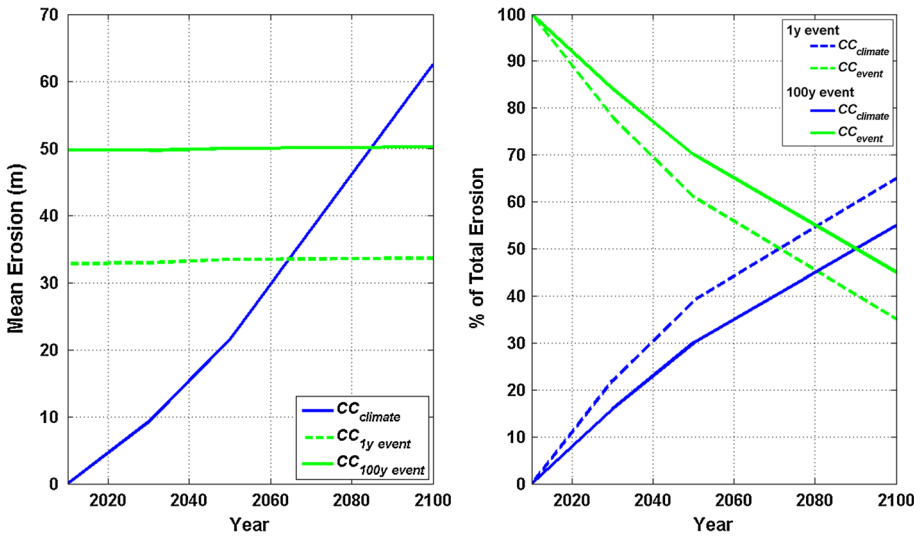


Fig. 7 County-wide average of mean coastal retreat, in meters, resulting from increasing sea levels ($CC_{climate}$; blue) versus the annual ($CC_{1y\ event}$; green dashed) and 100-year ($CC_{100y\ event}$; green solid) annual chance TWL events through 2100 (left) as well as the relative percent of total retreat of each coastal change component (right)

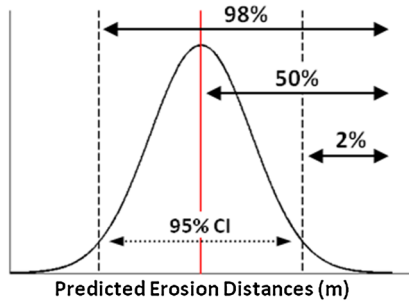
contribution to the total coastal change until shoreline retreat due to rising sea levels becomes the dominant factor late in the twenty-first century (Fig. 7). While dependent on our choice of dune erosion model (K99 is a conservative model), it is interesting that this shift occurs around 2070 for the annual return TWL event and not until 2090 for the 100-year event.

7 Coastal change hazard zones

At each time period of interest and for both of the extreme TWL events that have been chosen, 2,000 estimates for the total magnitude of coastal change were calculated. Dune erosion associated with the annual and 100-year TWL events for 2009, 2030, 2050, and 2100 presented here serve only as an example of the extreme events and time periods that can be analyzed, and different planning horizons and event extremities could be used by coastal planners. Regardless of the event chosen, the cross-shore distribution of the resulting coastal change estimates is highly alongshore-variable based on the local beach morphology. After examining hundreds of distributions, it was determined that a normal distribution was characteristic of most of them (Fig. 8). By assuming a normal distribution of the coastal change estimates, the results can be statistically summarized with the philosophy that decision makers have the option of choosing the level of risk they are willing to accept or what confidence level should trigger a particular policy option. Here, the 95 % confidence interval for the magnitude of change expected by a certain time period is defined as the mean and ± 2 standard deviations around the mean.

The raw coastal change estimates predicted from the simple models are highly variable in the alongshore due to the high-resolution of the lidar dataset from which the calculations

Probability of Exceedance:



Hazard Zones:

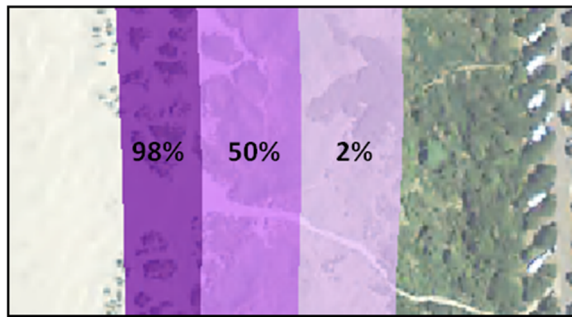


Fig. 8 Conceptual diagram illustrating the delineation of the CCHZs, which are defined probabilistically based on the 95 % confidence interval (CI) for the cross-shore distribution of expected coastal retreat distances

are based. Presenting the data in this way could exhibit too much variation for coastal planning purposes; therefore, the alongshore varying coastal change lines are smoothed with a quadratic loess filter to eliminate variability less than 250 m (Plant et al. 2002).

In addition to the increase in magnitude of the total coastal change hazards throughout the century, there is also an increase in the uncertainty associated with the calculations of expected coastal change. This increase has direct implications for the estimated impacts to coastal communities and shoreline properties because the hazard zones are ultimately defined based on these statistics. From the smoothed, alongshore varying coastal change distances for the mean and 95 % confidence interval, a suite of coastal change hazard zones were defined based on the probability of retreat exceeding a certain distance. In other words, there is a 98 % probability that the actual retreat will be greater than the mean -2σ , a 50 % probability it will be greater than the mean, and only a 2 % probability that the magnitude of retreat will be greater than the mean $+2\sigma$ (Fig. 8). The two landward most zones, therefore, compose the 95 % confidence interval within which the retreat for a given year and TWL event is most likely to achieve. The seaward edge of the 98 % exceedance probability zone is the alongshore-smoothed position of the 2002 lidar-derived dune toe.

The zones delineating various probabilities of coastal change exceedance provide decision makers with the ability to select probabilities that best match their risk tolerance. For example, an emergency manager may have a low-risk tolerance for life loss or other impacts to individuals and therefore use the most conservative zone delineating the 2 % exceedance. In contrast, a public works official deciding on the placement or upkeep of coastal infrastructure may have a higher risk tolerance than the emergency manager and may therefore be content using only the 50 % exceedance zone.

With these considerations in mind, coastal change hazard zones were developed for all dune-backed beaches of the four littoral cells in Tillamook County, for the annual and 100-year return level TWL events in 2009, 2030, 2050, and 2100. Mapped coastal change hazard zones take into account local geology (i.e., retreat was not allowed to cut through bluffs and erosion-resistant uplands), but do not take into account existing shore protection structures (e.g., riprap). Both the magnitude of predicted coastal change and the width of the hazard zones increase through time as the hazard become more severe and the uncertainty increases.

8 Variations in community exposure

Variations in the exposure of coastal communities to future coastal change hazards were estimated by integrating the physical model-based coastal change estimates with geospatial structure data using geographic information system software. The location of structures was derived based on the manual interpretation of 2009 aerial imagery (NAIP 2009) and on field reconnaissance. Results indicate that the number of structures in our study area potentially exposed to coastal change hazards increases throughout the century but these increases are not spatially consistent (Fig. 9). Note that here we are not modeling changes in development patterns or population distributions in Tillamook County and assume that the future landscape has the same number and spatial distribution of infrastructure and structures. Therefore, any estimated changes in societal exposure forecasted for the twenty-first century are due to climate change impacts alone. Planned work will integrate scenarios of land change and population demand (e.g., Sleeter et al. 2012) with the coastal hazard zones outlined in this paper. Related, further research will examine the influence of shore protection structures and the potential role of future adaptation strategies on reducing societal exposure to coastal change hazards on the Oregon coast.

The Rockaway littoral cell contains the greatest number of structures that are in coastal change hazard zone, both today and in the future. In 2009, there were 281 and 534 structures in coastal change hazard zones associated with the annual and 100-year TWL events, respectively. By the year 2050, the number of potentially exposed structures are more than doubles to 536 (793) structures due to the annual (100-year) TWL event and then to 968 (1116) structures by 2100. The Neskowin and Sand Lake littoral cells have far fewer structures within the hazard zones; however, the communities in these cells are much smaller than the City of Rockaway Beach and may sustain more significant losses as a whole. The fewest impacts to structures will be in the Netarts littoral cell because there is no coastal development along Netarts Spit, except for campground facilities in Cape Lookout State Park.

Trends of increased exposure through time will be a common theme throughout coastal areas, especially those that are heavily developed close to the shoreline. As the amount of forecasted coastal change increases so will the impact to adjacent infrastructure, depending on the community's spatial distribution and density. The relative impact of these hazards

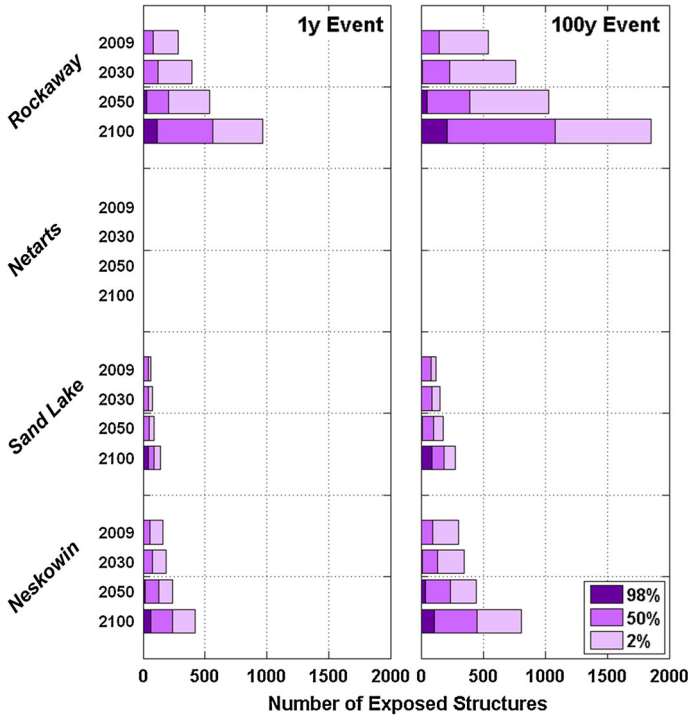


Fig. 9 Number of structures within the CCHZs through time for all littoral cells of Tillamook County associated with the 98, 50, and 2 % exceedance probabilities. The medium and light purples (50 and 2 % exceedance probabilities) indicate the 95 % confidence interval for the number of structures likely to be impacted

will depend on the community’s size and resilience, with smaller communities potentially being more sensitive to coastal infrastructure damage or loss. Methods outlined here to characterize the magnitude, uncertainty, and spatial variability of coastal hazard zones, as well as potential changes in structures exposure to these hazards, provide land-use planners and emergency managers with insight on potential changes in and implications of societal vulnerability over time. This information can serve as a critical input in the development of land-use scenarios, comprehensive land-use plans, resource management plans, and capital-improvement plans that each seeks to balance community development with long-term sustainability and resilience.

9 Influence of model components on coastal change hazards

We first assessed the relative contribution of sea level, wave climate, and the frequency of occurrence of major El Niños to the hazard zones by isolating the impact of the 20 individual scenarios using extreme TWLs in the Neskowin littoral cell in 2050. Standard deviations for each of the scenarios are small (less than ~0.5 m), implying that there is relatively minimal variability in the TWLs that result from the 100 different morphological configurations. We conducted a sensitivity analysis by investigating the relative impact of

Table 2 Relative impact of SLR, wave climate, and El Niño scenario ranges alone, with the other two components held constant, on the total predicted coastal change, expressed in terms of magnitude and percent increase (%) from the lowest to highest projection

TWL event	Year	Sea-level rise		Wave climate		El Niño frequency	
		Magnitude (m)	%	Magnitude (m)	%	Magnitude (m)	%
100 % annual chance	2030	7.3	18	2.8	6	0.1	0
	2050	15.6	33	5.7	10	1.1	2
	2100	42.7	63	6.0	7	1.4	2
1 % annual chance	2030	7.1	13	3.8	6	0	0
	2050	15.9	25	7.5	10	0	0
	2100	42.6	51	6.7	6	0	0

each one of the climate controls on the extreme TWLs by holding two of the three climate controls constant and comparing the extreme TWL values between the low and high projections of the third component. Based on the differences for all sets of projections and averaging the results, variability in the TWL based on the wave height scenarios has more of an impact on the extreme TWLs (0.4 m) than does the variability in the SLR scenarios (0.2 m) or the El Niño scenarios (<0.1 m).

The magnitude of forecasted coastal change also increases with increasing sea level and wave height projections, where total retreat distances range from 43.8 ± 22.9 m (59.1 ± 27.9 m) for the lowest scenario, LLM (Fig. 2c), to 66.1 ± 25.8 m (82.1 ± 29.7 m) for the highest scenario, HHH, for the annual (100-year) TWL events (Eq. 1). The range of SLR projections contributes more to the total variability in the magnitude of retreat (CCR_{climate}) than does the range of projections for wave climate (CC_{event}), regardless of the time period of interest (Table 2), which is counter to the results looking at influences on extreme TWLs. The reason the smaller change in the TWL results in a bigger change in the estimated retreat for the SLR scenarios is that the SLR component of the TWLs is divided by the shallow shoreface slope ($\tan \beta_{\text{sf}}$), using the equation for CC_{climate} (Eq. 2). In contrast, dividing the event component of the TWL by steeper backshore beach slopes ($\tan \beta_{\text{bs}}$), as is the case for CC_{event} (Eq. 6), results in relatively smaller retreat distances.

For example, scenarios involving the high SLR projection result in 15.9 m of additional erosion, on average, associated with the 100-year TWL event in 2050 over those involving the low SLR projection (Eq. 1). This corresponds to a 25 % increase in the magnitude of retreat between scenarios involving the low versus high SLR projections when wave height and El Niño scenarios are held constant (Table 2). For the same year and TWL event, the total coastline retreat predicted for scenarios involving the high wave climate projection, where wave heights are allowed to increase through the year 2030, is only 7.5 m greater (equivalent to a 10 % increase) than the scenarios with the low projection where wave heights decrease over the same time period. Because the total predicted retreat increases significantly between 2050 and 2100 but the range in the wave height scenarios stays relatively the same (since wave heights were only allowed to increase until 2030), the relative percentage decreases over time.

Doubling the frequency of El Niño events in the future, however, does not have a significant impact on the width of the hazard zones. The magnitude of erosion predicted for the 100-year return TWL event is insensitive to a doubling in the frequency

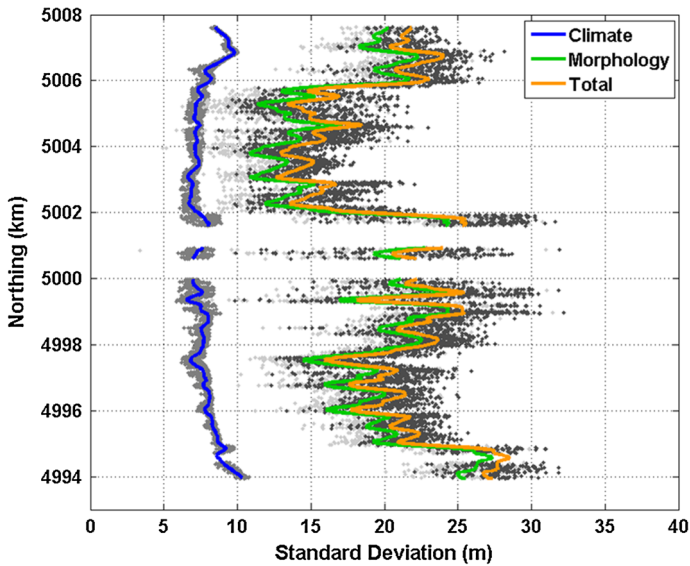


Fig. 10 Variability in coastal retreat estimates due to climate (*blue*) versus morphology (*green*) and the total variability of these uncertainties combined (*orange*) associated with the annual TWL event in 2050 for the Neskowin littoral cell

of El Niño, and the annual return TWL event only increases the total predicted retreat by 2 %. These results may be due to the fact that while this scenario brings the total number of major El Niños to four every 30 years, it modifies waves and water levels for only a few months approximately every 15 years. Therefore, the TWLs between the climate change scenarios with and without a doubling of El Niños are quite similar.

To determine which parameter is contributing more to the overall width of the coastal hazard zones, we examined the relative influence of uncertainty associated with climate change and morphological variability. Because the hazard zone width—or landward extent—is defined using the 95 % confidence interval in erosion modeling results, this can be done by comparing the alongshore varying standard deviations of each component. For one configuration of morphological parameters (i.e., the alongshore varying mean beach slope and dune toe elevation), the alongshore average standard deviation of the 20 climate change scenarios around the mean is found to be ~ 7.8 m (Fig. 10). In contrast, the standard deviation of the set of 100 iterations of morphology around any given climate change scenario is ~ 18.3 m, on average, which is more than double that of the uncertainty due to climate alone. Figure 10 illustrates how the standard deviation of both components varies alongshore for the Neskowin littoral cell, and how they compare to the standard deviation of all 2,000 erosion estimates combined. Based on these sensitivity analyses, morphological variability is more important than the uncertainty associated with the range of climate change scenarios applied here in determining the width of the coastal hazard zones. As statistical theory suggests, the total uncertainty (orange line in Fig. 10) results from the quadrature addition of the climate (blue line) and morphological (green line) uncertainties.

10 Conclusions

Our probabilistic method of quantifying and mapping coastal change hazards for a variety of dune-backed environments incorporates a range of projections for SLR, wave climate, and El Niño frequency, recognizes the uncertainty and variability associated with the impact of future climate change on extreme water levels and coastal change, and accounts for morphological variability. Rather than imposing one set of hazard zones on a local government, the approach presented here allows for decision makers to choose the level of risk they are willing to accept as well as what time period and design event for which they would like to develop adaptation plans. Results demonstrate that, despite significant uncertainties, coastal change hazards are likely to increase in the future and that community exposure to these hazards varies substantially. In order to most accurately portray the potential impacts of climate change on coastlines, one must consider not only SLR but also changes in storminess which can play a large role in the extreme water levels experienced at the shoreline and can cause increased episodic erosion of protective foredunes.

Acknowledgments The authors gratefully acknowledge the support of NOAA's Climate Program Office Sectoral Applications Research Program (SARP) under NOAA Grant #NA08OAR4310693, NOAA's Climate Program Office Coastal and Ocean Climate Applications Program under NOAA Grant #NA12OAR4310109, NOAA's National Sea Grant College Program under NOAA Grant #NA06OAR4170010, the Climate Impacts Research Consortium (CIRC) funded under NOAA Grant #NA10OAR4310218, and the US Geological Survey Land Change Science Program.

Open Access This article is distributed under the terms of the Creative Commons Attribution License which permits any use, distribution, and reproduction in any medium, provided the original author(s) and the source are credited.

References

- Allan JC, Komar PD (2000) Are ocean wave heights increasing in the eastern North Pacific? *EOS Trans AGU* 81(47):561–567
- Allan JC, Komar PD (2002) Extreme storms on the Pacific Northwest coast during the 1997–98 El Niño and 1998–99 La Niña. *J Coast Res* 18(1):175–193
- Allan JC, Komar PD (2006) Climate controls on U.S. West Coast erosion processes. *J Coast Res* 22:511–529
- Allan JC, Priest GR (2001) Evaluation of coastal erosion hazard zones along dune and bluff backed shorelines in Tillamook County, Oregon: Cascade Head to Cape Falcon Rep. Open File Report O-01-03, Oregon Department of Geology and Mineral Industries, Newport, OR
- Allan JC, Ruggiero P, Roberts JT (2012) Coastal flood insurance study, Coos County, Oregon. Oregon Department of Geology and Mineral Industries Special Paper 44, 119 pp
- Bindoff NL, Willebrand J, Artale V, Cazenave A, Gregory J, Gulev S, Hanawa K, Le Q, Levitus S, Nojiri Y, Shum CK, Talley LD, Unnikrishnan A (2007) Observations: oceanic climate change and sea level. In: Solomon S, Qin D, Manning M, Chen Z, Marquis M, Averyt KB, Tignor M, Miller HL (eds) *Climate change 2007: the physical science basis*. Contribution of Working Group I to the Fourth Assessment Report of the Intergovernmental Panel on Climate. Cambridge University Press, Cambridge
- Bruun P (1962) Sea-level rise as a cause of shore erosion. *J Waterw Harbors Div* 88:117–130
- Burgette RJ, Weldon RJ, Schmidt DA (2009) Interseismic uplift rates for western Oregon and along-strike variation in locking on the Cascadia subduction zones. *Geophys Res Lett* 114:B01408. doi:[10.1029/2008JB005679](https://doi.org/10.1029/2008JB005679)
- Cai W, Borlace S, Lengaigne M, van Rensch P, Collins M, Vecchi G, Timmermann A, Santoso A, McPhaden MJ, Wu L, England MH, Wang G, Guilyardi E, Jin F (2014) Increasing frequency of extreme El Niño events due to greenhouse warming. *Nat Clim Change* 4:111–116
- Callaghan DP, Nielsen P, Short A, Ranasinghe R (2008) Statistical simulation of wave climate and extreme beach erosion. *Coast Eng* 55(5):375–390

- Coles SG (2001) An introduction to statistical modeling of extreme values. Springer, London, p 208
- Cooper WS (1958) Coastal Sand Dunes of Oregon and Washington. *Memoirs of the Geological Society of America* (Boulder, Colorado). Memoir 72, pp 1–6
- Frazier TG, Wood N, Yarnal B, Bauer DH (2010) Influence of potential sea level rise on societal vulnerability to hurricane storm-surge hazards, Sarasota County, Florida. *App Geogr* 30(4):490–505. doi:10.1016/j.apgeog.2010.05.005
- Hemer MA, Fan Y, Mori N, Semedo A, Wang XL (2013) Projected changes in wave climate from a multi-model ensemble. *Nat Clim Change* 3(5):471–476
- Kaminsky GM, Ruggiero P, Gelfenbaum G (1998) Monitoring coastal change in southwest Washington and northwest Oregon during the 1997/98 El Niño. *Shore Beach* 66(3):42–51
- Komar PD, McDougall WG, Marra JJ, Ruggiero P (1999) The rational analysis of setback distances: applications to the Oregon coast. *Shore Beach* 67(1):41–49
- Komar PD, Allan JC, Ruggiero P (2011) Sea level variations along the U.S. Pacific Northwest coast: tectonic and climate controls. *J Coast Res* 27(5):808–823
- Kriebel DL, Dean RG (1993) Convolution method for time-dependent beach-profile response. *J Waterw Port Coast Ocean Eng* 119(2):204–226
- Larson M, Erikson L, Hanson H (2004) An analytical model to predict dune erosion due to wave impact. *Coast Eng* 51(8–9):675–696
- Méndez FJ, Menéndez M, Luceño A, Losada IJ (2006) Estimation of the long-term variability of extreme significant wave height using a time-dependent Peak Over Threshold (POT) model. *J Geophys Res Oceans* 111:C07024. doi:10.1029/2005JC003344
- Menéndez M, Méndez FJ, Losada IJ, Graham N (2008) Variability of extreme wave heights in the northeast Pacific Ocean based on buoy measurements. *Geophys Res Lett* 35:L22607. doi:10.1029/2008GL035394
- Mull J, Ruggiero P (2014) Estimating storm-induced dune erosion and overtopping along U.S. West Coast beaches. *J Coast Res*. doi:10.2112/JCOASTRES-D-13-00178.1
- NAIP (2009) Oregon 2009 half-meter color orthoimagery. National Agriculture Imagery Program, U.S. Department of Agriculture. <http://imagery.oregonexplorer.info/>. Accessed 1 June 2010
- National Research Council (2012) Sea-level rise for the coasts of California, Oregon, and Washington: Past, Present, and Future. Committee on Sea Level Rise in California, Oregon, and Washington; Board on Earth Sciences and Resources; Ocean Studies Board; Division on Earth and Life Studies
- NDBC (2007) National Data Buoy Center, National Oceanographic and Atmospheric Administration. <http://seaboard.ndbc.noaa.gov/>. Accessed 1 June 2010
- NOAA (2007) National Oceanographic and Atmospheric Administration <http://tidesandcurrents.noaa.gov/sltrends/sltrends.shtml>. Accessed 1 June 2010
- NOAA Center for Tsunami Research (2004) Central Oregon, OR 6 arc-second MHW Tsunami Inundation DEM. NOAA's National Geodetic Data Center (NGDC). <http://www.ngdc.noaa.gov/mgg/inundation/82>. Accessed 18 Nov 2010
- NOAA Coastal Services Center (2002) 2002 NASA/USGS Airborne LiDAR Assessment of Coastal Erosion (ALACE) Project for California, Oregon, and Washington Coastlines. NOAA's Ocean Service, Coastal Services Center (CSC). <http://www.csc.noaa.gov/ldart>
- Plant NG, Holland KT, Puelo JA (2002) Analysis of the scale of errors in nearshore bathymetric data. *Mar Geol* 191:71–86
- Rahmstorf S (2010) A new view on sea level rise. *Nature* 4:44–45
- Revell DL, Battalio R, Spear B, Ruggiero P, Vandever J (2011) A methodology for predicting future coastal hazards due to sea-level rise on the California coast. *Clim Change* 109:S251–S276. doi:10.1007/s10584-011-0315-2
- Ruggiero P (2013) Is the intensifying wave climate of the U.S. Pacific Northwest increasing flooding and erosion risk faster than sea-level rise? *J Waterw Port Coast Ocean Eng* 139(2):88–97
- Ruggiero P, List JH (2009) Improving accuracy and statistical reliability of shoreline position and change rate estimates. *J Coast Res* 25(5):1069–1081
- Ruggiero P, Kaminsky GM, Gelfenbaum G, Voigt B (2005) Seasonal to interannual morphodynamics along a high-energy dissipative littoral cell. *J Coast Res* 21(3):553–578
- Ruggiero P, Komar PD, McDougal WG, Marra JJ, Beach RA (2001) Wave runup, extreme water levels and the erosion of properties backing beaches. *J Coast Res* 17(2):407–419
- Ruggiero P, Komar PD, Allan JC (2010) Increasing wave heights and extreme-value projections: the wave climate of the U.S. Pacific Northwest. *Coast Eng* 57:539–552. doi:10.1016/j.coastaleng.2009.12.005
- Ruggiero P, Kratzmann MA, Himmelstoss EG, Reid D, Allan J, Kaminsky G (2013) National assessment of shoreline change: historical shoreline change along the Pacific Northwest Coast. U.S. Geological Survey Open-File Report 2012–1007, 55 p

- Sallenger AH (2000) Storm impact scale for barrier islands. *J Coast Res* 16(3):890–895
- Sleeter BM, Sohl TL, Bouchard MA, Reker RR, Soulard CE, Acevedo W, Griffith GE, Sleeter RR, Auch RF, Sayler KL, Prisley S, Zhu Z (2012) Scenarios of land use and land cover change in the conterminous United States: utilizing the special report on emission scenarios at ecoregional scales. *Glob Environ Change* 22:896–914
- Stockdon HF, Holman RA, Howd PA, Sallenger AH Jr (2006) Empirical parameterization of setup, swash, and runup. *Coast Eng* 53:573–588
- Strauss BH, Ziemlinski R, Weiss JL, Overpeck JT (2012) Tidally adjusted estimates of topographic vulnerability to sea level rise and flooding for the contiguous United States. *Environ Res Lett* 7:014033. doi:[10.1088/1748-9326/7/1/014033](https://doi.org/10.1088/1748-9326/7/1/014033)
- Thieler ER, Hammar-Klose ES (1999) National assessment of coastal vulnerability to sea-level rise, U.S. Atlantic coast. U.S. Geological Survey Open-File Report 99-593
- Wilby RL, Dessai SD (2012) Robust adaptation to climate change. *Weather* 65(7):180–185
- Wu SY, Najjar R, Siewert J (2009) Potential impacts of sea-level rise on the mid- and upper-Atlantic Region of the United States. *Clim Change* 95:121–138. doi:[10.1007/s10584-008-9522-x](https://doi.org/10.1007/s10584-008-9522-x)
- Young I, Zieger S, Babanin A (2011) Global trends in wind speed and wave height. *Science* 332(6028):451–455